Inertia Decoupling Identification Strategy Based on Disturbance Torque Adaptive Observation for PMSM Drives

Yuanming Huang, Guoqiang Zhang, *Senior Member, IEEE*, Gaolin Wang, *Senior Member, IEEE*, Qiwei Wang, *Member, IEEE*, Siqi Wang, and Dianguo Xu, *Fellow, IEEE*

***Abstract*—The acceleration errors generated during the speed sampling process decrease the inertia identification accuracy of permanent magnet synchronous motor (PMSM) drives under low acceleration conditions. This article proposes an inertia decoupling identification strategy based on disturbance torque adaptive observation for PMSM drives. By revealing the impacts of acceleration errors, the relationship among the sampling windows, the inertia identification error, and the disturbance torque observation error is obtained. On this basis, the sampling windows for the inertia identification and the disturbance torque observation are adaptively adjusted under different speed and acceleration conditions, which expands the application range of inertia identification. Besides, according to the coupling characteristics between the inertia and the disturbance torque, an adaptive linear neuron network-based iterative mechanism is constructed. The inertia identification and disturbance torque observation can be iteratively updated, which improves the inertia decoupling identification accuracy. The stability and convergence are analyzed in detail. The experimental results verify the effectiveness of the proposed method.**

***Index Terms*—Adaptive linear neuron network (ADALINE), inertia decoupling identification, low acceleration conditions, permanent magnet synchronous motor (PMSM), sampling windows adaptive adjustment.**

I. Introduction

PERMANENT magnet synchronous motor (PMSM), known for its high efficiency, high power density, and high torque inertia ratio, has been widely applied in the fields of rail transit, industrial manufacturing, and energy conversion [1], [2]. The control performance of PMSM is related to the inertia when using the field-oriented control method [3], [4]. Mismatched system inertia would lead to the deterioration of PMSM's speed control performance [5], [7]. Besides, under low acceleration conditions, there arises a further challenge in the inertia identification accuracy. Therefore, it is essential to investigate effective inertia identification methods under different operating conditions.

The implementation of the inertia identification relies on the acceleration calculated by the differentiation of speed under a fixed sampling window. However, the limited speed measurement resolution and the quantization error would lead to the acceleration sampling errors [8], [9], [10]. The impacts of the acceleration errors are significant under low acceleration conditions [11], [12], which result in an inaccurate inertia identification. Therefore, the inertia identification is mostly carried out under higher acceleration conditions to ensure identification accuracy.

According to the above issues, on the one hand, the signal injection methods could be adopted to identify the inertia, avoiding the need for speed differentiation. In [13], the inertia could be obtained from the position of the zero-crossing point and the amplitude and frequency of the sine speed signal. A sinusoidal current signal with dc bias was adopted in [14], which avoided the discontinuity of the electromagnetic torque during the process of inertia identification. In [15], both the inertia and the friction were obtained at a sinusoidal low frequency speed by integrating the torque in a half period. In general, the signal injection methods are applicable when the motor is under no-load or relatively fixed load conditions.

On the other hand, the online processing algorithms could be adopted to reduce the acceleration errors. In [16], an extended moving window was adopted to calculate polynomial functions, which could reduce noise interference in speed differentiation at low speeds. In [17], the low-pass filters were adopted for speed and torque filtering, reducing the speed measurement error and improving the inertia identification accuracy. The acceleration-based disturbance observer was designed to avoid the quadratic differentiation of position in [18]. The analysis of the acceleration errors generated during the encoder speed sampling process was deficient. In [19], a variable period shaping method was proposed, which could reduce the quantization error of the speed measurement method. In [20], a variable period inertia identification strategy was proposed to improve the inertia identification accuracy of the integration method under low acceleration conditions. However, the impacts of the acceleration errors on the disturbance torque observation are rarely

Received 31 October 2024; accepted 31 December 2024. Date of publication 7 January 2025; date of current version 26 February 2025. This work was supported in part by the Research Fund for the National Natural Science Foundation of China under Grant 52177034 and Grant 52125701, in part by the Heilongjiang Provincial Natural Science Foundation under Grant YQ2023E016, in part by the Aeronautical Science Foundation of China under Grant ASFC-20220007077002, and in part by the Fundamental Research Funds for the Central Universities under Grant HIT.OCEF.2023003. Recommended for publication by Associate Editor K. Akatsu. *(Corresponding author: Qiwei Wang.)*

The authors are with the School of Electrical Engineering and Automation, Harbin Institute of Technology, Harbin 150001, China (e-mail: huangym@stu.hit.edu.cn; zhgq@hit.edu.cn; wgl818@hit.edu.cn; wqw0543@163.com; 21b906039@stu.hit.edu.cn; xudiang@hit.edu.cn).

Color versions of one or more figures in this article are available at https://doi.org/10.1109/TPEL.2025.3526610.

Digital Object Identifier 10.1109/TPEL.2025.3526610

investigated. The relationship among the acceleration errors, the disturbance torque observation, and the inertia identification needs further research.

Additionally, since the inertia identification is influenced by the disturbance torque including the friction torque and the load torque, it is necessary to achieve the inertia decoupling identification. Due to rank-deficient problem in the mechanical equation, the number of parameters identified simultaneously cannot exceed one [21]. In [22] and [23], the friction coefficient, the inertia, and the load torque were identified separately in multiple steps at different speed trajectories, which could obtain all parameters in the motor mechanical equation and avoid the rank-deficient problem. In [24], the multiple interconnected sliding mode observer networks were proposed to achieve iterative identification among the friction coefficient, the inertia, and the load torque. In [25], the friction torque was calculated offline under no-load conditions, and a proportional-integral regulator was adopted to adjust the disturbance torque and the inertia estimation error to achieve simultaneous identification. In order to reduce the complexity of the identification system, by defining the constraint that the derivative of the disturbance torques is zero, the disturbance torque could be identified as a lumped parameter. In [26] and [27], the constant disturbance torque derivative is constructed as the constraint of the observer to ensure stability and convergence under steady-state conditions. However, the actual disturbance torque is a function of the speed. The constraint of constant disturbance torque derivative cannot be satisfied under transient conditions. The designed disturbance torque observer has the problem of estimating oscillations [28], which will affect the observation of disturbance torque under transient conditions and the accuracy of inertia decoupling identification.

This article proposes an inertia decoupling identification strategy based on disturbance torque adaptive observation for PMSM drives. The contributions mainly include the following.

1) The relationship among the acceleration errors, the inertia identification error, and the disturbance torque observation error is investigated. Based on the sampling process of speed measurement under low acceleration conditions, the impacts of the acceleration errors are revealed. Besides, the coupling characteristics are constructed to elucidate the relationship between inertia and disturbance torque.
2) The sampling windows adaptive adjustment strategy is proposed for low acceleration conditions. The sampling windows for the inertia identification and the disturbance torque observation are adaptively adjusted under different speed and acceleration conditions, improving the accuracy of the inertia identification and the disturbance torque observation under low acceleration conditions.
3) The iterative mechanism based on adaptive linear neuron (ADALINE) network is proposed to achieve decoupling identification. The iterative mechanism is constructed by the ADALINE network and updated with different update periods, avoiding the oscillation of disturbance torque observation and decoupling the coupling effects between parameters. Besides, the stability and convergence of the proposed method are analyzed by Lyapunov functions and state equations.

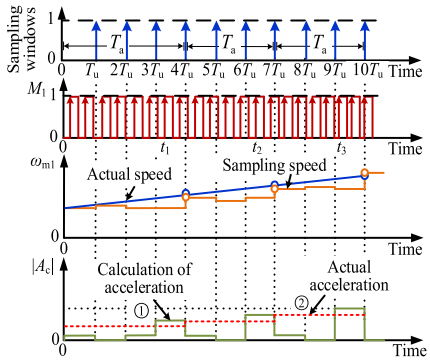

Fig. 1. Sampling analysis result under low acceleration condition.

II. Error Analysis of Inertia Identification Under Low Acceleration Conditions

A. Analysis of Inertia Identification Affected by Acceleration Errors

The mechanical equation of PMSM under $i_d = 0$ control can be expressed as

$$T_e - T_L = J\frac{d\omega_m}{dt} + B\omega_m \tag{1}$$

$$\frac{3}{2}n_p\psi_f - T_L = \frac{J}{n_p}\frac{d\omega_e}{dt} + \frac{B}{n_p}\omega_e \tag{2}$$

where T_e and T_L are the electromagnetic torque and the load torque, respectively. J, B, ω_m, ω_e, n_p, and ψ_f are the system inertia, the friction coefficient, the mechanical angular speed, the electric angular speed, the pole pairs, and the flux linkage, respectively. The load torque and the friction torque can be concentratedly expressed as the disturbance torque, which is $T_d = B\omega_m + T_L$.

The mechanical angular speed in (1) can be calculated by M/T method. The number of pulses output by the encoder and the high-frequency clock signal are M_1 and M_2, respectively, which are simultaneously recorded within sampling window T_u. When M_2 changes, the speed resolution R_1 under low-speed conditions can be expressed as

$$R_1 = \frac{2\pi f_0 M_1}{N(M_2-1)} - \frac{2\pi f_0 M_1}{NM_2} = \frac{2\pi f_0 M_1}{NM_2(M_2-1)} \tag{3}$$

where N is the resolution of the encoder and f_0 is the frequency of the high frequency clock signal.

In the higher speed region, M_2 remains basically unchanged, that is, $M_2 \approx f_0 T_u$. Hence, the speed resolution R_2 under high-speed conditions can be expressed as

$$R_2 = \frac{2\pi f_0 M_1}{NM_2} - \frac{2\pi f_0 (M_1-1)}{NM_2} = \frac{2\pi}{NT_u}. \tag{4}$$

The speed measurement quantization error E_q of the encoder can be expressed as

$$E_q = R_1 = \frac{N\omega_m^2}{2\pi f_0 M_1 - N\omega_m}. \tag{5}$$

Fig. 1 shows the sampling analysis result of the motor speed under low acceleration condition, which is $\omega_m(k+T_u)$

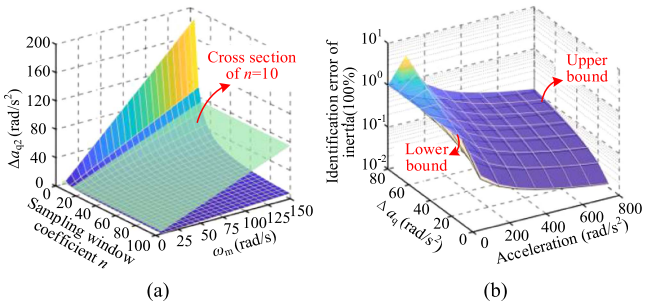

Fig. 2. Analysis result of the acceleration errors and the inertia identification error. (a) Relationship among Δa_{q2}, n, and ω_m. (b) Relationship among the inertia identification error, Δa_q, and the acceleration.

$-\omega_m(k) < R_1$ or R_2, $k < T_a - T_u$. Where T_a are the sampling windows for actual speed, ω_{m1} is the sampling speed, t_1, t_2, and t_3 are the update time of the sampling speed. $|A_c|$ is the absolute of the acceleration. As can be seen from Fig. 1, the deviation of sampling speed from the actual speed is mainly affected by two factors: one is the limited speed measurement resolution of the encoder, and the other is the speed quantization error. If the measurement resolution is limited, it is difficult to detect the slight changes of speed, resulting in the output of the encoder pulse lagging behind the changes of the actual speed. Besides, the sampling speed is affected by the quantization error under the fixed sampling window T_u. The sampling speed deviates from the actual speed, resulting in speed fluctuations. As can be seen from curve ①, the absolute value of the calculated acceleration, which is $|d\omega_m/dT_u|$, deviates from the actual value curve ②.

Based on the above analysis, the total acceleration errors Δa_q can be expressed as

$$\Delta a_q = \Delta a_{q1} + \Delta a_{q2} \tag{6}$$

where Δa_{q1} and Δa_{q2} are the acceleration errors, which are caused by the limited measurement resolution and the quantization error, respectively.

The relationship between the sampling window T_u and the carrier period T_s is defined as $T_u = nT_s$ $(n > 1)$, where n is the sampling window coefficient. The acceleration error caused by speed measurement quantization error can be expressed as

$$\Delta a_{q2} = \frac{E_q}{T_u} = \frac{N{\omega_m}^2}{nT_s(2\pi f_0 M_1 - N\omega_m)}. \tag{7}$$

Fig. 2(a) shows the analysis result of the acceleration error Δa_{q2}, which reveals the relationship among the acceleration error, the sampling window coefficient, and the mechanical angular speed. When the fixed sampling window is set to $n = 10$, the acceleration error caused by the quantization error is proportional to the mechanical angular speed. When the mechanical angular speed is constant, as the sampling window coefficient increases, Δa_{q2} decreases.

According to the analysis above, the inertia identification considering the acceleration errors can be expressed as

$$\hat{J} = \frac{T_e - T_\mathrm{d}}{\frac{d\omega_m}{dT_u} \pm \Delta a_q} \tag{8}$$

where the superscript "^" is the estimation of the variable. As can be seen in (8), the inertia identification relies on the feedback speed rather than the given speed. If the speed feedback cannot follow the given sine speed signal, the inertia still can be identified through the feedback speed. However, due to the poor dynamic performance caused by the lower speed controller bandwidth, the operating state of the motor may be under low acceleration conditions. The proportion of acceleration errors in the denominator term is relatively small under high acceleration conditions, and the inertia identification error is also small. When the acceleration of operating speed is small, the proportion of acceleration errors in the denominator term is relatively large in (8), resulting in significant errors of inertia identification. In addition, as the operating speed of the motor increases, the total acceleration errors increase due to the increase of Δa_{q2}.

When the disturbance torque is accurate, the maximum inertia identification error considering the influence of the acceleration errors can be expressed as

$$\begin{aligned}\Delta\hat{J}_{\max} &= \max\left\{\left|\frac{\frac{T_e-T_d}{\frac{d\omega_m}{dT_u}} - \frac{T_e-T_d}{\frac{d\omega_m}{dT_u}\pm\Delta a_q}}{\frac{T_e-T_d}{\frac{d\omega_m}{dT_u}}}\right|\right\} \\ &= \max\left\{\left|1 - \frac{\frac{d\omega_m}{dt}}{\frac{d\omega_m}{dt} \pm \Delta a_q}\right|\right\}\end{aligned} \tag{9}$$

where $\Delta\hat{J}_{\max}$ is the maximum inertia identification error, the function "max{}" denotes the maximum value.

As shown in Fig. 2(b), the relationship among the inertia identification error, the acceleration errors, and the acceleration is revealed. The inertia identification error is logarithmically processed for analysis. The inertia identification error increases when Δa_q increases. However, as the acceleration increases, the upper and lower bounds of the inertia identification error gradually decrease. Thus, in order to reduce the inertia identification error, it needs to be identified under higher acceleration conditions, which limits the operating range.

B. Coupling Characteristics Analysis Between Inertia and Disturbance Torque

According to the mechanical equation of PMSM, the implementation of the inertia identification requires the known disturbance torque. However, the disturbance torque observation is also affected by acceleration errors, resulting in the inertia decoupling identification errors.

Thus, the maximum disturbance torque estimation error considering the influence of the acceleration errors can be expressed as

$$\begin{aligned}\Delta\hat{T}_{d\max} &= \max\left\{\left|\frac{T_e - J\frac{d\omega_m}{dT_u} - \left(T_e - \hat{J}\left(\frac{d\omega_m}{dT_u} \pm \Delta a_q\right)\right)}{T_e - J\frac{d\omega_m}{dT_u}}\right|\right\} \\ &= \max\left\{\left|\frac{(\hat{J} - J)\cdot\frac{d\omega_m}{dT_u} \pm \hat{J}\Delta a_q}{T_d}\right|\right\}\end{aligned} \tag{10}$$

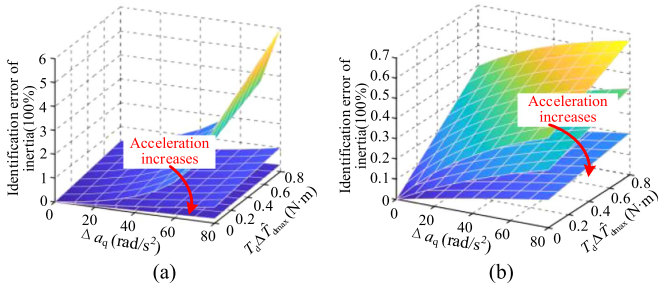

Fig. 3. Error analysis result of the inertia decoupling identification. (a) Upper bound. (b) Lower bound.

where $\Delta\hat{T}_{d\max}$ is the maximum disturbance torque estimation error.

According to (10), since there is a significant error in inertia identification under low acceleration condition, the disturbance torque observation error increases. Similarly, the disturbance torque observation error caused by the acceleration errors will lead to the deterioration of the inertia identification, which causes the coupling effect. Thus, the maximum inertia identification error considering the disturbance torque observation error can be further rewritten as

$$\Delta\hat{J}_{\max} = \max\left\{\left|1-\frac{\frac{d\omega_m}{dT_u}}{\frac{d\omega_m}{dT_u}\pm\Delta a_q}\cdot\frac{T_e-(T_d\pm T_d\Delta\hat{T}_{d\max})}{T_e-T_d}\right|\right\} \tag{11}$$

where $T_d\Delta\hat{T}_{d\max}$ is the absolute error of the disturbance torque observation.

Fig. 3 shows the error analysis result of the inertia decoupling identification. As can be seen, as Δa_q and $T_d\Delta\hat{T}_{d\max}$ increase, the upper and lower bounds of the inertia decoupling identification error gradually increase. Besides, as the acceleration of the motor increases, the upper and lower bounds of the inertia decoupling identification error gradually decrease. Based on the above analysis, it can be seen that the increase of the disturbance torque observation error caused by the acceleration errors led to the further restriction of operating acceleration.

III. Proposed Inertia Decoupling Identification Strategy Based on Disturbance Torque Adaptive Observation

A. Adaptive Adjustment Strategy for Sampling Windows

The proposed inertia decoupling identification strategy based on disturbance torque adaptive observation is shown in Fig. 4. The proposed method mainly includes the adaptive adjustment strategy for sampling windows and the ADALINE-based iterative mechanism to achieve inertia decoupling identification. By setting the expected thresholds of the inertia identification error and the absolute error of the disturbance torque observation, the sampling windows for the inertia identification algorithm are adaptively adjusted by the criteria of the limited measurement resolution and the quantization error. Besides, the sampling windows for the disturbance torque observation algorithm are adaptively adjusted by the inertia identification. Considering the coupling characteristics between the inertia and the disturbance torque, an ADALINE-based iterative mechanism is constructed to decouple the mutual influence of parameter identifications.

The discretized mechanical equations can be expressed as

$$\omega_m(k)=\omega_m(k-1)+\frac{T_s}{J(k)}\left[T_e(k)-T_d(k)\right] \tag{12}$$

where k represents the discrete sampling moment.

Since ADALINE network has the advantages of simple computation and adaptive adjustment [29], the inputs, the output, and the weights of (12) can be constructed as

$$\underbrace{\hat{\omega}_m(k)}_{\text{Output1}}=\underbrace{\omega_m(k-1)}_{I_{p1}}\cdot\underbrace{1}_{W_1}+\underbrace{T_s\left[T_e(k)-\hat{T}_d(k)\right]}_{I_{p2}}\cdot\underbrace{\frac{1}{\hat{J}(k)}}_{W_2} \tag{13}$$

where I_{p1} and I_{p2} are the input signals and W_1 and W_2 are the weights.

According to the resolution between adjacent speed update times, the limited measurement resolution R_r of the encoder can be expressed as

$$R_{\mathrm{r}}=\frac{2\pi f_0(M_1+1)}{NM_2^*}-\frac{2\pi f_0M_1}{NM_2} \tag{14}$$

where M_2^* is the output pulses of the high-frequency clock signal when the output pulses of the encoder are M_1+1. Therefore, R_r can be calculated by the encoder output pulse M_1 and the high-frequency clock pulse M_2.

As shown in (15), when the sampling speed meets the limited resolution criterion, the sampling window can be adjusted to T_u'

$$|\omega_m(k)-\omega_m(k-T_u')|\geq R_r. \tag{15}$$

Taking into account the quantization error, the maximum inertia identification error can be expressed as

$$\Delta\hat{J}_{\max}=\max\left\{\left|1-\frac{dR_r/dT_u'}{dR_r/dT_u'\pm\Delta a_{q2}}\right|\right\} \tag{16}$$

where T_u' is the sampling window after adaptively adjusting by the limited measurement resolution.

By defining $dR_r/dT_u'=\Delta a_{q2}/E_d$ and $0<E_d<1$, the inertia identification error can be further expressed as

$$\Delta\hat{J}_{\max}=\max\left\{\left|1-\frac{1}{1-E_d}\right|,\left|1-\frac{1}{1+E_d}\right|\right\}=\frac{E_d}{1-E_d} \tag{17}$$

where E_d is the acceleration error coefficient.

According to (17), the maximum inertia identification error can be controlled by the expected threshold of $\Delta\hat{J}_{\max}$.Then, E_d can be expressed as

$$E_d=\frac{\Delta\hat{J}_{\max}}{1+\Delta\hat{J}_{\max}}. \tag{18}$$

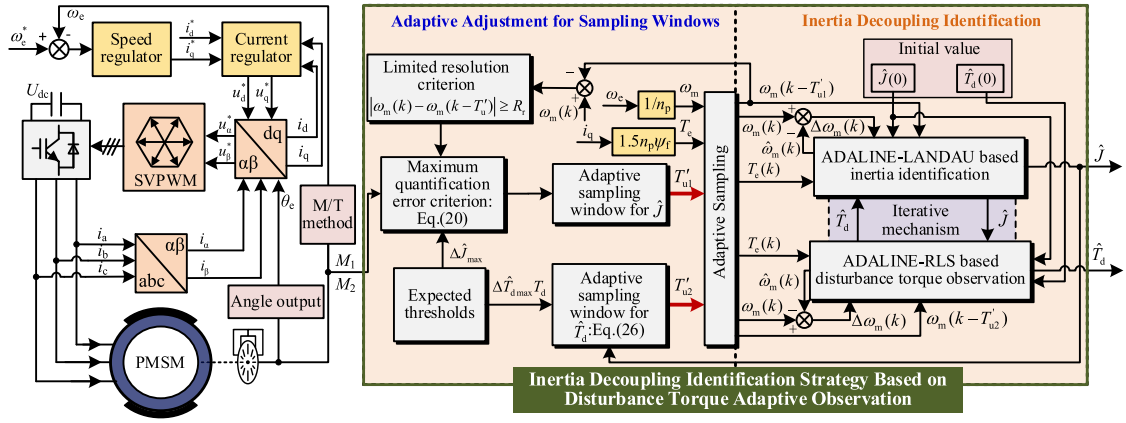

Fig. 4. Block diagram of the inertia decoupling identification strategy based on disturbance torque adaptive observation.

According to (18), the constraint condition of the acceleration can be expressed as

$$A \geq \frac{\Delta a_{q2}}{E_d} = \frac{\left(1+\Delta\hat{J}_{\max}\right)\Delta a_{q2}}{\Delta\hat{J}_{\max}} = \frac{\left(1+\Delta\hat{J}_{\max}\right)N{\omega_m}^2}{\Delta\hat{J}_{\max}(2\pi f_0 M_1 - N\omega_m)T'_{u1}} \tag{19}$$

where A is the acceleration of the motor, T'_{u1} is the sampling window after adaptively adjusting by the quantization error.

According to (19), the criterion of the speed difference under T'_{u1} can be expressed as

$$\begin{cases} |\omega_m(k) - \omega_m(k-T'_{u1})| \geq \frac{\left(1+\Delta\hat{J}_{\max}\right)N{\omega_m}^2}{\Delta\hat{J}_{\max}(2\pi f_0 M_1 - N\omega_m)} \\ T'_{u1} \leq T'_{u1\_\max} \end{cases} \tag{20}$$

where $T'_{u1\_\max}$ is the maximum constraint of T'_{u1}.

Based on the above analysis, the sampling windows can be adaptively adjusted according to (20). By using the Landau integral adaptive rate to update the inertia identification, the ADALINE-LANDAU inertia identification is expressed as

$$\begin{cases} \underbrace{\hat{\omega}_m(k)}_{\text{Output1}} = \underbrace{\omega_m(k-T'_{u1})}_{I_{p1}} \cdot \underbrace{1}_{W_1} + \underbrace{T'_{u1}\left[T_e(k) - \hat{T}_d(k)\right]}_{I_{p2}} \cdot \underbrace{\frac{1}{\hat{J}(k)}}_{W_2} \\ \frac{1}{\hat{J}(k+T'_{u1})} = \frac{1}{\hat{J}(k)} + \frac{\delta I(k)}{\left[T'_{u1}+\delta I^2(k)\right]}\Delta\omega_{\mathrm{m}}(k) \end{cases} \tag{21}$$

where $I(k) = I_{p2}(k)$, $\Delta\omega_m(k) = \omega_m(k) - \hat{\omega}_m(k)$. δ is the coefficient of integral gain. As the δ increases, the convergence step increases, with an increased noise interference in I_{p2}.

The total torque fluctuation can be expressed as

$$\Delta\tilde{T}(k) = \tilde{T}_e(k) + \tilde{T}_d(k) \tag{22}$$

where $\Delta\tilde{T}(k)$ is the total torque fluctuation, $\tilde{T}_e(k)$ is the electromagnetic torque error caused by sampling noise, $\tilde{T}_d(k)$ is the disturbance torque observation error.

According to (21) and (22), the inertia identification can be further expressed as

$$\begin{aligned} \frac{1}{\hat{J}(k+T'_{u1})} &= \frac{1}{\hat{J}(k)} + \frac{\delta I(k)}{[T'_{u1}+\delta I^2(k)]}\frac{T'_{u1}}{\hat{J}(k)}\Delta\tilde{T}(k) \\ &= \frac{1}{\hat{J}(k)}\left(1+\Delta\frac{1}{\tilde{J}(k)}\right) \end{aligned} \tag{23}$$

where $\Delta\frac{1}{\tilde{J}(k)} = \frac{1}{\tilde{J}(k)} - \frac{1}{\hat{J}(k)}$, $\tilde{J}(k)$ is the inertia identification affected by fluctuations.

The fluctuation variation of inertia identification can be expressed as

$$\begin{aligned} \left|\Delta\frac{1}{\tilde{J}(k)}\right| &= \delta\frac{T'_{u1}\left|\Delta\tilde{T}(k)\right|}{\left|\frac{T'_{u1}}{I(k)}\right| + \delta\left|I(k)\right|} \\ &\leq \frac{\delta}{2}\left|\Delta\tilde{T}(k)\right|. \end{aligned} \tag{24}$$

As shown in (24), the inertia identification fluctuation is related to the integral gain coefficient δ and $\Delta\tilde{T}(k)$. Therefore, the selection of δ could be configured based on the threshold of the inertia identification fluctuation and the total torque fluctuation to balance the convergence speed and the identification effectiveness. The design of δ can be expressed as

$$\frac{2\left|\Delta\frac{1}{\tilde{J}}\right|}{\left|\Delta\tilde{T}\right|_{\max}} \leq \delta \leq \frac{2\left|\Delta\frac{1}{\tilde{J}}\right|}{\left|\Delta\tilde{T}\right|_{\min}} \tag{25}$$

where $|\Delta\tilde{T}|_{\max}$ and $|\Delta\tilde{T}|_{\min}$ are the maximum and the minimum of the total torque fluctuations absolute value, respectively.

In order to reduce the impact of acceleration errors on disturbance torque observation, combining with (10), the sampling window for the disturbance torque observation can be adaptively adjusted as

$$\begin{cases} T'_{u2} = \frac{\hat{J}E_{q\max}}{\Delta\hat{T}_{d\max}T_d} = \frac{\hat{J}\omega_{m\max}}{\Delta\hat{T}_{d\max}T_d\ (f_0T_u-1)} \\ T'_{u2} \leq T'_{u2\_\max} \end{cases} \tag{26}$$

where T'_{u2} is the sampling window for the disturbance torque observation, $E_{q\max}$ is the maximum of the quantization error,

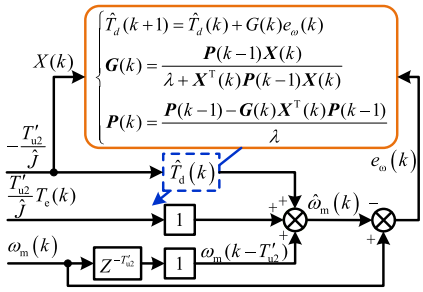

Fig. 5. Block diagram of the disturbance torque observer based on ADALINE network.

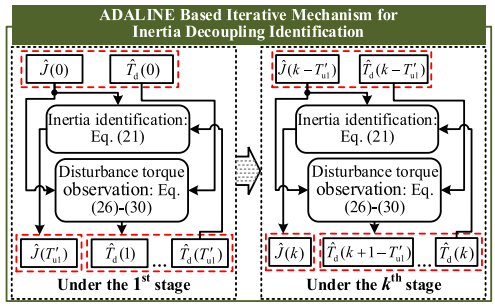

Fig. 6. ADALINE-based iterative mechanism for inertia decoupling identification.

$\omega_{m\max}$ is the maximum speed, and $T'_{u2\_\max}$ is the maximum constraint of T'_{u2}. By setting the absolute error of the disturbance torque observation, the sampling window for disturbance torque observation is adaptively adjusted in the process of inertia identification, which could improve the accuracy of disturbance torque observation and the accuracy of inertia decoupling identification.

B. ADALINE-Based Iterative Mechanism for Inertia Decoupling Identification

The block diagram of the disturbance torque observer based on ADALINE network is shown in Fig. 5. Similarly, the inputs, the output, and the weights of the disturbance torque observation can be expressed as

$$\underbrace{\hat{\omega}_m(k)}_{\text{Output2}} = \underbrace{\omega_m(k-T'_{u2})}_{x_{p1}}\cdot\underbrace{1}_{W_3}+\underbrace{\frac{T'_{u2}}{\hat{J}(k)}T_e(k)}_{x_{p2}}\cdot\underbrace{1}_{W_4} \underbrace{-\frac{T'_{u2}}{\hat{J}(k)}}_{x_{p3}}\cdot\underbrace{\hat{T}_d(k)}_{W_5} \tag{27}$$

where x_{p1}, x_{p2}, and x_{p3} are the inputs, W_3, W_4, and W_5 are the weights.

By using the recursive least squares (RLS) with forgetting factor to update the adjustable weight W_5 as

$$\hat{T}_d(k+1)=\hat{T}_d(k)+G(k)e_\omega(k) \tag{28}$$

where $e_\omega(k)=\omega_m(k)-\hat{\omega}_m(k)$. The gain vector $\boldsymbol{G}(k)$ can be expressed as

$$\boldsymbol{G}(k)=\frac{\boldsymbol{P}(k-1)\boldsymbol{X}(k)}{\lambda+\boldsymbol{X}^T(k)\boldsymbol{P}(k-1)\boldsymbol{X}(k)} \tag{29}$$

where λ is the forgetting factor and $\boldsymbol{X}(k)$ is the input vector.

The inverse of the autocorrelation matrix $\boldsymbol{P}(k)$ is

$$\boldsymbol{P}(k)=\frac{\boldsymbol{P}(k-1)-\boldsymbol{G}(k)\boldsymbol{X}^T(k)\boldsymbol{P}(k-1)}{\lambda}. \tag{30}$$

According to the error between the actual output and the target output, the disturbance torque observation is adaptively adjusted by the RLSs with forgetting factor to achieve convergence of the algorithm. The constraint of constant disturbance torque derivative is not applied in the construction of the proposed disturbance torque observer, avoiding the problem of oscillation observation.

Since the number of parameters identified simultaneously cannot exceed the rank of the mechanical equation, an inertia decoupling identification iterative mechanism is proposed to solve the rank-deficient problem in Fig. 6. Fig. 6 shows the detailed internal structure of ADALINE-based iterative mechanism in Fig. 4, describing the decoupling iterative update process of inertia and disturbance torque with different update periods. Since the variation rate of the disturbance torque is not zero, the actual observed disturbance torque cannot be reflected through excessive update period. Therefore, the update period of the disturbance torque observation is set to be consistent with the update period of the system interruption.

The iterative update process of solving the coupling problem between inertia and disturbance torque is analyzed as follows. Under the first stage of iterative updates, when $k=0$ in (27) and (28), the disturbance torque observation can be expressed as

$$\begin{cases}\hat{\omega}_m(0)=\omega_m(0-T'_{u2})\cdot 1+\frac{T'_{u2}}{\hat{J}(0)}T_e(0)\cdot 1-\frac{T'_{u2}}{\hat{J}(0)}\cdot\hat{T}_d(0)\\ \hat{T}_d(1)=\hat{T}_d(0)+G(0)e_\omega(0)\end{cases} \tag{31}$$

When $k=0\sim(T'_{u1}-1)$, the inertia remains at $\hat{J}(0)$, and the disturbance torque observation $\hat{T}_d(1)\ldots\hat{T}_d(T'_{u1})$ can be obtained by the ADALINE-RLS algorithm. At the T'_{u1} moment, (21) could be substituted into $\hat{T}_d(T'_{u1})$ to reformulate. Since the inertia still remains at $\hat{J}(0)$, the estimated speed in (21) can be expressed as

$$\hat{\omega}_m(T'_{u1})=\omega_m(0)\cdot 1+T'_{u1}\left[T_e(T'_{u1})-\hat{T}_d(T'_{u1})\right]\cdot\frac{1}{\hat{J}(0)}. \tag{32}$$

By the ADALINE-LANDAU algorithm, the updated inertia identification $\hat{J}(T'_{u1})$ can be expressed as

$$\frac{1}{\hat{J}(T'_{u1})}=\frac{1}{\hat{J}(0)}+\frac{\delta I(T'_{u1})}{[T'_{u1}+\delta I^2(T'_{u1})]}\Delta\omega_m(T'_{u1}). \tag{33}$$

Similarly, under the kth stage of iterative updates, the disturbance torque observation $\hat{T}_d(k+1-T'_{u1})\ldots\hat{T}_d(k)$ can be obtained at $(k-T'_{u1})\sim(k-1)$ moments. At the k moment, (21) can be substituted into $\hat{T}_d(k)$ to reformulate. Since the inertia still remains at $\hat{J}(k-T'_{u1})$, the estimated speed in (21) can be expressed as

$$\hat{\omega}_m(k)=\omega_m(k-T'_{u1})\cdot 1+T'_{u1}\left[T_e(k)-\hat{T}_d(k)\right]\cdot \times\frac{1}{\hat{J}(k-T'_{u1})}. \tag{34}$$

Here, $\hat{T}_d(k)$ is used for iteration to obtain $\hat{J}(k)$, achieving the inertia decoupling identification. The updated inertia identification $\hat{J}(k)$ can be expressed as

$$\frac{1}{\hat{J}(k)} = \frac{1}{\hat{J}(k-T'_{u1})} + \frac{\delta I(k)}{[T'_{u1}+\delta I^2(k)]}\Delta\omega_m(k). \tag{35}$$

In summary, the decoupling between the disturbance torque and the inertia can be achieved through the proposed iterative mechanism.

C. Analysis of Stability and Convergence

The identification errors of the inertia and the disturbance torque are defined as

$$\begin{cases} \varepsilon_j(k) = \frac{1}{J} - \frac{1}{\hat{J}(k)} \\ \varepsilon_d(k) = T_d - \hat{T}_d(k) \end{cases} \tag{36}$$

where ε_j and ε_d are the identification errors of the inertia and the disturbance torque, respectively.

According to (21), (27), and (36), the speed estimation errors can be calculated as

$$\begin{cases} e_{j\omega}(k) = \omega_m(k) - \omega_m(k-T'_{u1}) - \frac{1}{\hat{J}(k)}I(k) \\ \qquad = I(k)(\frac{1}{J} - \frac{1}{\hat{J}(k)}) = I(k)\varepsilon_j(k) \\ e_{d\omega}(k) = \omega_m(k) - \omega_m(k-T'_{u2}) - \frac{T'_{u2}}{J}T_e(k) + \frac{T'_{u2}}{J}\hat{T}_d(k) \\ \qquad = x_{p3}\left[T_d - \hat{T}_d(k)\right] = x_{p3}\varepsilon_d(k) \end{cases} \tag{37}$$

where $e_{j\omega}$ and $e_{d\omega}$ are the speed estimation errors of the ADALINE-LANDAU and the ADALINE-RLS algorithms, respectively.

As can be seen from (37), the speed errors could be expressed as the product of the input vector and the state vector. Therefore, according to the error term of the state vector in the speed error expression, the square of the error term is constructed as a Lyapunov function. The Lyapunov functions are constructed as

$$V(k) = \varepsilon_j(k)^2 + \varepsilon_d(k)^2 \tag{38}$$

where $V(k)$ are the Lyapunov functions of the ADALINE-LANDAU and the ADALINE-RLS algorithms.

The construction method not only meets the requirement of positive-definite function, but also includes the simplification operation of the speed error term in the differential calculation process. According to the Lyapunov stability principle, the difference of $V(k)$ can be calculated as

$$\begin{aligned} \Delta V(k) &= \left[\frac{1}{J} - \frac{1}{\hat{J}(k+T'_{u1})}\right]^2 - \varepsilon_j^2(k) \\ &\quad + \left[T_d - \hat{T}_d(k+1)\right]^2 - \varepsilon_d(k)^2 \\ &= \left[\varepsilon_j(k) - \frac{\delta I(k)}{[T'_{u1}+\delta I^2(k)]}e_{j\omega}(k)\right]^2 - \varepsilon_j^2(k) \\ &\quad + [\varepsilon_d(k) - G(k)e_{d\omega}(k)]^2 - \varepsilon_d(k)^2 \\ &= \psi I(k)\varepsilon_j^2(k)(-2+\psi I(k)) + G(k)x_{p3}\varepsilon_d(k)^2 \\ &\quad \times (-2+G(k)x_{p3}) \end{aligned} \tag{39}$$

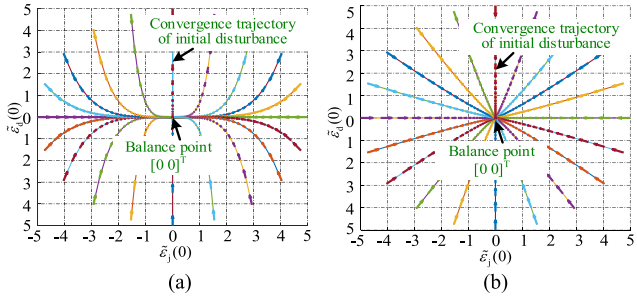

Fig. 7. Trajectory variations of identification errors. (a) $\psi = 0.4$, $G(k)x_{p3} = 1.8$. (b) $\psi = 0.8$, $G(k)x_{p3} = 0.9$.

where $\Delta V(k)$ is the difference of $V(k)$, $\psi = \frac{\delta I(k)}{[T'_{u1}+\delta I^2(k)]}$.

Since $0 < \psi I(k) < 1$ and $0 < G(k)x_{p3} < 1$, $\Delta V(k) < 0$ when $\varepsilon_j(k) \neq 0$ and $\varepsilon_d(k) \neq 0$. It can be concluded that the ADALINE-LANDAU inertia identification and the ADALINE-RLS disturbance torque observation is always stable. It means that the inertia identification error and the disturbance torque observation error could converge to zero, and they are not affected by the initial values. Besides, the constraint of constant disturbance torque derivative is not existed in the construction and stability analysis of the proposed disturbance torque observer, avoiding the problem of oscillation observation.

Based on the stability analysis of the system, the identification error variations of the inertia and the disturbance torque for its convergence can be obtained as

$$\begin{cases} \frac{d\varepsilon_j(k)}{dt} = -\alpha e_{j\omega}(k) = -\alpha I(k)\varepsilon_j(k) \\ \frac{d\varepsilon_d(k)}{dt} = B\frac{de_{d\omega}(k)}{dt} - \beta e_{d\omega} = Bx_{p3}\frac{d\varepsilon_d(k)}{dt} - \beta x_{p3}\varepsilon_d(k) \end{cases} \tag{40}$$

where α and β are the identification coefficients.

According to (40), the state equations of the identification errors can be obtained as

$$\begin{bmatrix} \dot{\varepsilon}_j(k) \\ \dot{\varepsilon}_d(k) \end{bmatrix} = \begin{bmatrix} -\alpha I(k) & 0 \\ 0 & -\frac{\beta x_{p3}}{1-Bx_{p3}} \end{bmatrix} \begin{bmatrix} \varepsilon_j(k) \\ \varepsilon_d(k) \end{bmatrix} \tag{41}$$

where the superscript "$\cdot$" is the derivative of the variables.

According to (21) and (28), the corresponding relationship of the identification coefficients can be expressed as

$$\begin{cases} \alpha = \psi = \frac{\delta I(k)}{[T'_{u1}+\delta I^2(k)]} \\ \beta = (1-Bx_{p3})G(k) \end{cases}. \tag{42}$$

The initial disturbances are defined as

$$\begin{bmatrix} \tilde{\varepsilon}_j(0) \\ \tilde{\varepsilon}_d(0) \end{bmatrix} = \begin{bmatrix} 5\sin\delta \\ 5\cos\delta \end{bmatrix}, \quad 0 \le \delta \le 2\pi. \tag{43}$$

Fig. 7 shows the trajectory variations of identification errors with different coefficients. It can be seen that the identification errors of the inertia and the disturbance torque converge to zero in different trajectories under a large range of disturbances, and the inertia and disturbance torque can converge to real values from arbitrary initial values.

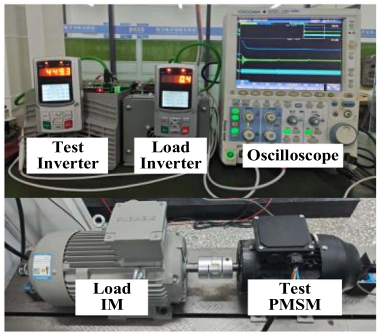

Fig. 8. Experimental platform of the 2.2 kW PMSM.

TABLE I
PMSM PARAMETERS

Parameter	Value	Parameter	Value
Rated power	2.2 kW	Pole pairs	3
Rated voltage	380 V	System inertia	0.0200 kg·m^2
Rated current	4.4 A	Flux linkage	0.5 Wb
Rated torque	14 N·m	Encoder resolution	8000 p/r
Rated speed	50 π rad/s	High frequency clock	2 MHz

IV. EXPERIMENTAL RESULTS

Fig. 8 shows the 2.2 kW PMSM platform used for verifying the effectiveness of the proposed strategy, and Table I gives the parameters of the motor. The total inertia of the system includes the inertia of the test PMSM, the load IM, and the coupling, which are 0.00381, 0.0149, and 1.3×10^{-3} kg·m^2, respectively. The total inertia of the system is calculated as 0.0200 kg·m^2. The ARM chip STM32F103 is used to implement the proposed strategy, which can quickly handle various complex algorithms and has a high cost performance ratio. The execution time of the proposed inertia decoupling identification strategy is 11.40 μs, which is much smaller than the PWM period 125 μs. The PWM carrier frequency is 8 kHz and the sampling window for the speed loop is 1.25 ms. The expected threshold of $\Delta\hat{J}_{\max}$ and $\Delta\hat{T}_{d\max}T_d$ is set to 5.0% and 0.3 N·m, respectively. To avoid prolonged identification time caused by excessively large sampling windows, $T'_{u1\_\max}$ and $T'_{u2\_\max}$ are set to 10 ms. In this article, the forgetting factor is set to 0.9993.

Fig. 9 shows the experimental comparisons of acceleration calculation between the fixed sampling window and the adaptive sampling windows under low acceleration conditions with an amplitude of 5 π rad/s and a frequency of 2 Hz at different speeds. It can be seen from Fig. 9(a) that compared with $|a_{r\_max}|$, the acceleration errors under the fixed sampling window (1.25 ms) gradually increases with the increase of the speed. Since the quantization error is relatively small at the speed of $5\pi + 5\pi\sin(4\pi t)$ rad/s, the acceleration accuracy is relatively high. However, some parts of the acceleration errors still reach 63.8π rad/s^2. At the speed of $25\pi + 5\pi\sin(4\pi t)$ rad/s, the acceleration errors increase significantly, with the maximum error reaching 80.6π rad/s^2. Thus, under the fixed sampling window, the acceleration accuracy cannot be guaranteed at different speeds. Fig. 9(b) shows the experimental results of the proposed adaptive sampling windows for sampling speed signals under the same speed condition as Fig. 9(a). As shown by the purple curve in Fig. 9(b), the adaptive values of sampling time are given. According to the criterion constraints of the limited measurement resolution and quantization error, the sampling window for the speed is adaptively adjusted under different speed and acceleration conditions based on the adaptive sampling windows. At the speed of $5\pi + 5\pi\sin(4\pi t)$ rad/s, the sampling window is adaptively adjusted, with a maximum up to 10 ms and a minimum up to 3 ms. At the speed of $25\pi + 5\pi\sin(4\pi t)$ rad/s, the minimum sampling window is adaptively adjusted to 4 ms. It can be seen that the maximum of the acceleration calculation remains within the range of $|a_{r\_\max}|$, with a relatively accurate acceleration at different speeds.

Fig. 10 shows the experimental comparisons of inertia identification under continuous speed variation and 0% rated load conditions, which consider the impacts of the acceleration errors. Fig. 10(a) shows the experimental results of inertia identification under the fixed sampling window. As shown in Fig. 10(a), at the speed of $5\pi+5\pi\sin(4\pi t)$ rad/s, the inertia identification value is 0.0216 kg·m^2, with an error of 8.0%. However, at the speed of $25\pi+5\pi\sin(4\pi t)$ rad/s, the inertia identification value is 0.0128 kg · m^2, with an error of 36.0%. The error has increased by 28% compared with the result at the speed of $5\pi+5\pi\sin(4\pi t)$ rad/s. The experimental results indicates that the inertia identification accuracy under low acceleration conditions cannot be ensured under the fixed sampling window. As the speed increases, the inertia identification accuracy deteriorates. Fig. 10(b) shows the experimental results of inertia decoupling identification under the adaptive sampling windows. The inertia identification experiments are carried out at the speed shown in Fig. 9(b), so the speed sampling windows of the inertia identification algorithm are consistent with those in Fig. 9(b). As shown in Fig. 10(b), as the speed increases, the inertia identification becomes stable. Based on the absolute error of the disturbance torque observation, the sampling window for disturbance torque observation is adaptively adjusted in the process of inertia identification, which is about 4 ms. At the speed of $5\pi + 5\pi\sin(4\pi t)$ rad/s, the inertia identification value is 0.0202 kg·m^2, with an error of 1.0%. At the speed of $25\pi + 5\pi\sin(4\pi t)$ rad/s, the inertia identification value is 0.0198 kg·m^2, with an error of 1.0%. According to the iterative mechanism, the disturbance torque observation can be reflected from inertia identification. Compared with the result under the fixed sampling window, the proposed adaptive sampling windows strategy improves the accuracy of the inertia identification and the disturbance torque observation under low acceleration conditions, keeping the inertia decoupling identification errors within 5.0%.

At the speed of $15\pi+5\pi\sin(4\pi t)$ rad/s and the load of 3.5 N·m, Fig. 11 shows the convergence experimental results of the inertia decoupling identification under different initial values. As can be seen from Fig. 11, the estimated values of inertia and disturbance torque can converge within 8 s under different initial values. The experimental results reveal that the estimated values of inertia and disturbance torque can approach the actual values without being affected by the initial values.

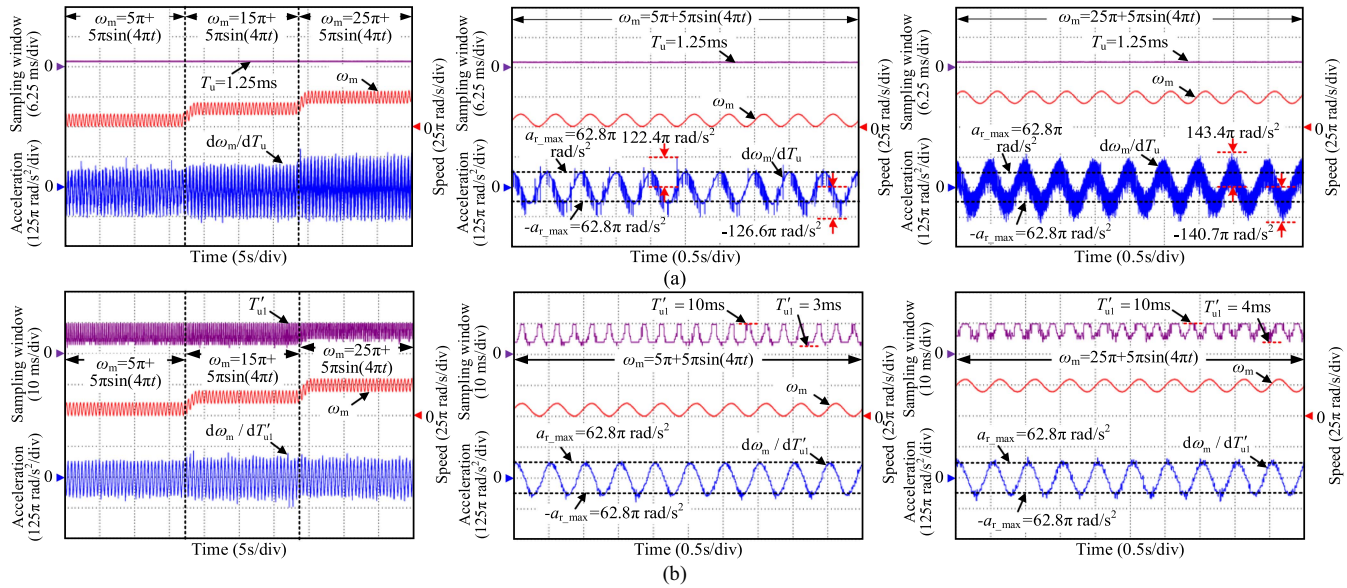

Fig. 9. Experimental comparisons of acceleration calculation under low acceleration at different speeds. (a) Fixed sampling window. (b) Adaptive sampling windows.

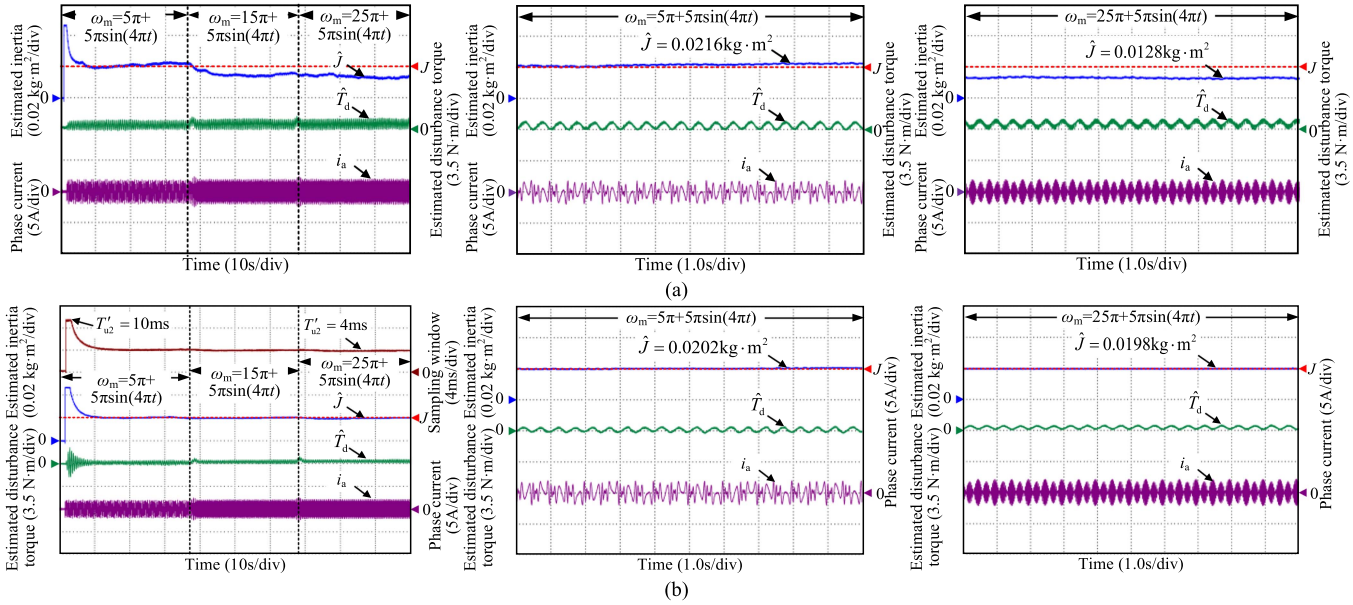

Fig. 10. Experimental comparisons of inertia identification under low acceleration at different speeds. (a) Fixed sampling window. (b) Adaptive sampling windows.

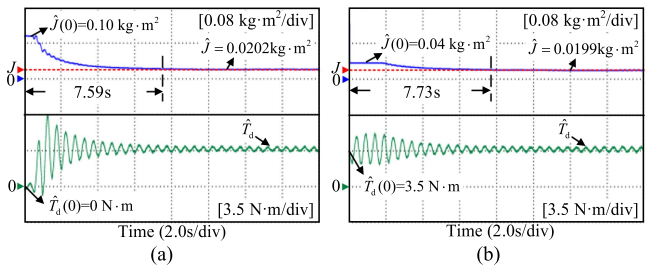

Fig. 11. Experiment results of the inertia decoupling identification under different initial values. (a) $\hat{J}(0) = 0.10\,\mathrm{kg\cdot m^2}$, $\hat{T}_\mathrm{d}(0) = 0\,\mathrm{N\cdot m}$. (b) $\hat{J}(0) = 0.04\,\mathrm{kg\cdot m^2}$, $\hat{T}_\mathrm{d}(0) = 3.5\,\mathrm{N\cdot m}$.

Fig. 12 shows the statistical experimental results of inertia identification at $25\pi+(5\pi+3.125m\pi)\sin(4\pi t)$ rad/s (m = 0-4 denotes five different accelerations), where the acceleration denotes the maximum acceleration of the sine speed. In Fig. 12, under the conventional strategy of fixed sampling window, as the acceleration increases, the inertia identification error decreases, from a maximum of 36.0% to a minimum of 0.5%. The inertia identification value with the largest error is $0.0128\,\mathrm{kg\cdot m^2}$. The inertia identification accuracy under high acceleration conditions is higher than that under low acceleration conditions, and the experimental results are consistent with the theoretical analysis. After adopting the proposed adaptive adjustment strategy

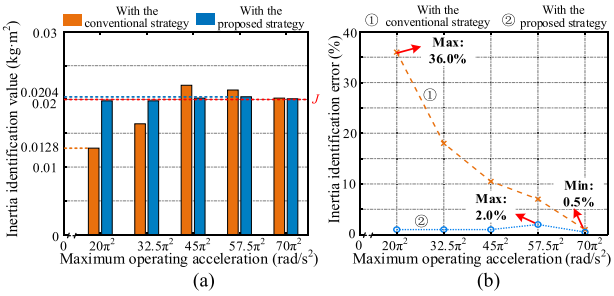

Fig. 12. Statistical experimental results of inertia identification under different acceleration conditions. (a) Inertia identification value. (b) Inertia identification error.

for sampling windows, the consistency of inertia identification under different acceleration conditions is improved, with the identification errors within 5.0%. The inertia identification value with the largest error is $0.0204\ \mathrm{kg\cdot m^2}$. The maximum identification error is 2.0%, which is 34% lower than that without the proposed strategy. The application range of inertia identification is expanded by the proposed strategy.

Considering the impacts of the disturbance torque observation on inertia identification under different load conditions and the influence of the acceleration errors on disturbance torque observation, Fig. 13 shows the experimental comparisons of inertia identification under different load conditions at low acceleration $(15\pi + 5\pi\sin(4\pi t)\,\mathrm{rad/s})$. Fig. 13(a) shows the experimental result of inertia identification without decoupling. It can be seen that as the disturbance torque increases, the inertia identification gradually shifts from the actual value during loading. The maximum error reaches the limitation of $0.05\,\mathrm{kg\cdot m^2}$ and the minimum error is 11.5%. Besides, the disturbance torque observation exhibits significant errors. The observation performance experiments of the reduced-order disturbance torque observer in [27] are carried out to further illustrate the main advantages of the proposed disturbance torque observer. By using the reduced-order disturbance torque observer, Fig. 13(b) shows the experimental results of inertia decoupling identification under different load conditions. As can be seen from Fig. 13(b), the reduced-order disturbance torque observer is affected by the constraint of constant disturbance torque derivative, resulting in observation oscillations under transient conditions. The maximum error of inertia identification is 39.5%. The experimental results indicate that the reduced-order disturbance torque observer exhibits oscillations under transient conditions, resulting in significant inertia identification errors. In order to further verify the influence of acceleration errors on disturbance torque observation. Fig. 13(c) shows the experimental result of inertia decoupling identification by using the conventional strategy that does not consider the effect of acceleration errors on disturbance torque observation. As can be seen in Fig. 13(c), the large acceleration errors under low acceleration conditions leads to the errors in the disturbance torque observation. From the perspective of identification accuracy of the inertia, it can be seen that the inertia identification error is above 10%, with a maximum of 17.0%. By using the proposed inertia decoupling identification strategy based on disturbance torque adaptive observation, Fig. 13(d) shows the experimental result of inertia

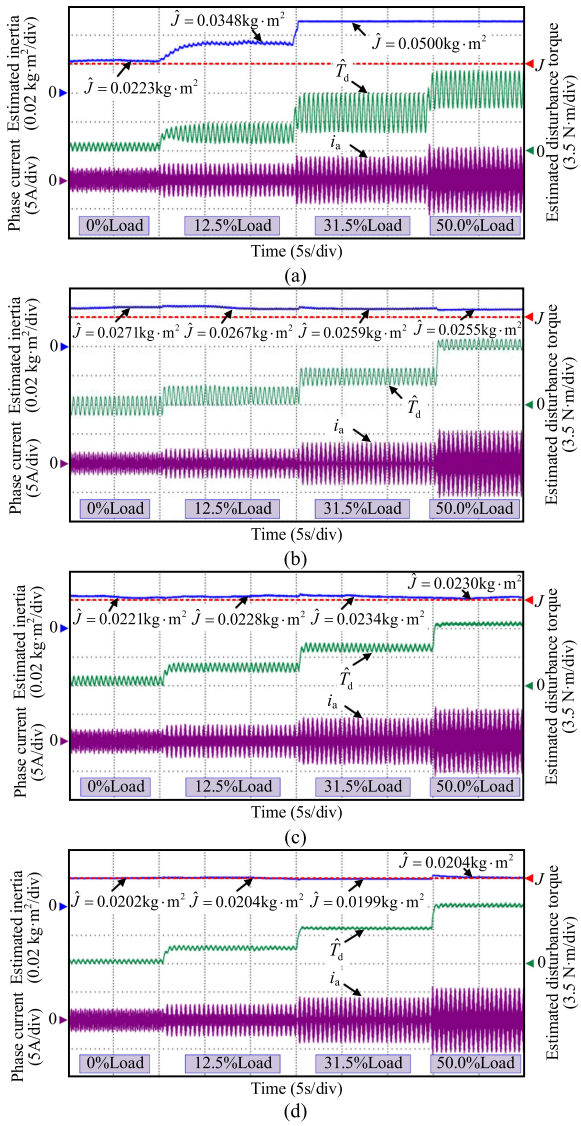

Fig. 13. Experimental comparisons of inertia identification under different load conditions at low acceleration. (a) Without decoupling. (b) With reduced-order disturbance torque observer. (c) Without considering the impacts of the acceleration errors. (d) Considering the impacts of the acceleration errors.

decoupling identification considering the effect of the acceleration errors on disturbance torque observation. As the disturbance torque increases, the inertia identification remains stable, with a high accuracy of over 95.0% and the maximum inertia identification error of 2.0%. Besides, the oscillations caused by the constraint of constant disturbance torque derivative are avoided. The effectiveness of the proposed strategy in inertia decoupling identification under different load conditions is further verified.

Fig. 14 shows the statistical experimental results of inertia identification under different speed and load conditions. The results reveal that the proposed strategy improves the impacts of acceleration errors on disturbance torque observation and avoids the constraint of constant disturbance torque derivative. The inertia decoupling identification accuracy under different speed and load conditions is enhanced, keeping the inertia decoupling identification errors under low acceleration conditions within 5.0%.

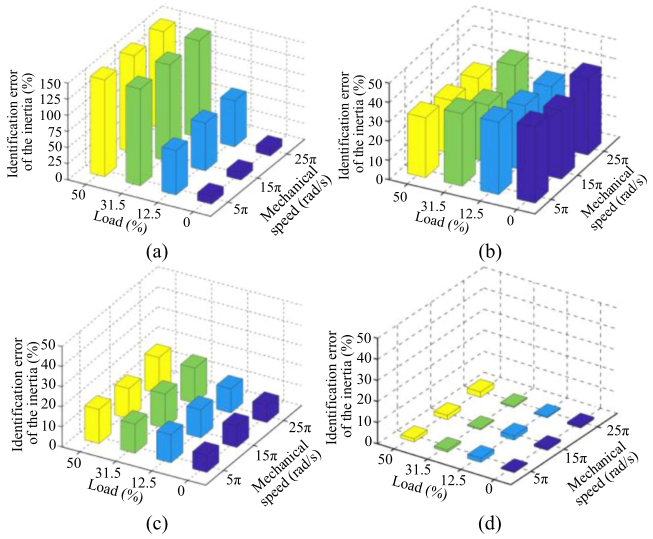

Fig. 14. Statistical experimental results of inertia identification under different speed and load conditions. (a) Without decoupling. (b) With reduced-order disturbance torque observer. (c) Without considering the impacts of the acceleration errors. (d) Considering the impacts of the acceleration errors.

V. Conclusion

This article proposes an inertia identification strategy based on disturbance torque adaptive observation for PMSM drives. By revealing the impacts of the acceleration errors, the relationship among the sampling windows, the inertia identification error, and the disturbance torque observation error is clarified. An adaptive adjustment strategy for sampling windows is proposed to reduce the acceleration errors and improve the accuracy of the inertia identification and the disturbance torque observation under low acceleration conditions. Besides, an ADALINE network-based iterative mechanism is constructed to decouple the mutual influence between the inertia and the disturbance torque, which improves the inertia decoupling identification accuracy. The experimental results reveal that the proposed method expands the acceleration application range of inertia identification and the inertia decoupling identification accuracy under low acceleration conditions at different speeds and loads can be maintained above 95.0%.

References

[1] W. Lu et al., "A new load torque identification sliding mode observer for permanent magnet synchronous machine drive system," *IEEE Trans. Power Electron.*, vol. 34, no. 8, pp. 7852–7862, Aug. 2019.

[2] Q. Wang, G. Wang, N. Zhao, G. Zhang, Q. Cui, and D. Xu, "An impedance model-based multiparameter identification method of PMSM for both offline and online conditions," *IEEE Trans. Power Electron.*, vol. 36, no. 1, pp. 727–738, Jan. 2021.

[3] G. Bi et al., "Multi-optimization objective online tracking-based parameter self-tuning method for sensorless PMSM drives," *IEEE Trans. Transp. Electrific.*, vol. 9, no. 1, pp. 1390–1402, Mar. 2023.

[4] Y. Zhang, X. Huang, A. Wang, and J. Xu, "A position and speed controller tuning method of permanent magnet synchronous linear motor based on gain identification," *IEEE Trans. Power Electron.*, vol. 37, no. 10, pp. 11716–11724, Oct. 2022.

[5] F. Erturk and B. Akin, "Inertia estimation and speed loop auto-tuning for IPMSM self-commissioning," *IEEE Trans. Energy Convers.*, vol. 34, no. 3, pp. 1706–1714, Sep. 2019.

[6] C. Hsu and Y. Lai, "Novel online optimal bandwidth search and autotuning techniques for servo motor drives," *IEEE Trans. Ind. Appl.*, vol. 53, no. 4, pp. 3635–3642, Jul./Aug. 2017.

[7] G. Wang, M. Valla, and J. Solsona, "Position sensorless permanent magnet synchronous machine drives—A review," *IEEE Trans. Ind. Electron.*, vol. 67, no. 7, pp. 5830–5842, Jul. 2020.

[8] T. Shi, Z. Wang, and C. Xia, "Speed measurement error suppression for PMSM control system using self-adaption Kalman observer," *IEEE Trans. Ind. Electron.*, vol. 62, no. 5, pp. 2753–2763, May 2015.

[9] X. Yang, Y. Guo, and H. Wang, "Encoder signal analysis and its application in gear fault detection," *IEEE Trans. Instrum. Meas.*, vol. 73, Dec. 2024, Art. no. 3505709.

[10] D. Wang, X. Liu, X. Wu, K. Xu, and J. Li, "Instantaneous angular speed extraction based on nonuniform local polynomial differentiator for the stiffness identification of the robot joint," *IEEE Trans. Instrum. Meas.*, vol. 72, Dec. 2023, Art. no. 6500110.

[11] Z. Zhou, S. Zhang, Z. Xu, Y. Peng, and X. Jin, "High-quality positioning strategy for biaxial contour machining system with nonlinear model predictive control," *IEEE J. Emerg. Sel. Topics Power Electron.*, vol. 11, no. 4, pp. 4355–4367, Aug. 2023.

[12] Y. Bai et al., "High-gain nonlinear active disturbance rejection control strategy for traction permanent magnet motor drives," *IEEE Trans. Power Electron.*, vol. 37, no. 11, pp. 13135–13146, Nov. 2022.

[13] K. Liu and Z. Zhu, "Fast determination of moment of inertia of permanent magnet synchronous machine drives for design of speed loop regulator," *IEEE Trans. Control Syst. Technol.*, vol. 25, no. 5, pp. 1816–1824, Sep. 2017.

[14] K. Liu, C. Hou, and W. Hua, "Novel inertia identification method and its application in PI controllers of PMSM drives," *IEEE Access*, vol. 7, pp. 13445–13454, Jan. 2019.

[15] S. Kim, "Moment of inertia and friction torque coefficient identification in a servo drive system," *IEEE Trans. Ind. Electron.*, vol. 66, no. 1, pp. 60–70, Jan. 2019.

[16] Y. Bai, G. Zhang, G. Wang, F. Chen, G. Bi, and D. Xu, "Position and speed detection method based on adaptive extended moving-window linear regression for traction machine drives," *IEEE Trans. Transp. Electrific.*, vol. 8, no. 2, pp. 2884–2897, Jun. 2022.

[17] Y. Zuo, J. Mei, X. Zhang, and C. H. T. Lee, "Simultaneous identification of multiple mechanical parameters in a servo drive system using only one speed," *IEEE Trans. Power Electron.*, vol. 36, no. 1, pp. 716–726, Jan. 2021.

[18] S. Fang, Y. He, P. Wan, and Z. Pan, "Low-speed control of arc motor using Kalman observer via acceleration-based disturbance observer," *IEEE Trans. Power Electron.*, vol. 39, no. 1, pp. 1254–1268, Jan. 2024.

[19] Y. Chen, M. Yang, D. Xu, and F. Blaabjerg, "A novel frequency characteristic model and noise shaping method for encoder-based speed measurement in motor drive," in *Proc. 10th Int. Conf. Power Electron. ECCE Asia*, 2019, pp. 1–6.

[20] Y. Chen, M. Yang, J. Long, W. Qu, D. Xu, and F. Blaabjerg, "A moderate online servo controller parameter self-tuning method via variable-period inertia identification," *IEEE Trans. Power Electron.*, vol. 34, no. 12, pp. 12165–12180, Dec. 2019.

[21] C. Yang, B. Song, J. Jatskevich, H. Zhang, and C. H. T. Lee, "Normal-operation-undisturbed magnet flux linkage monitoring in PMSM drives via a mechanical-model-based dual time-scale approach," *IEEE Trans. Ind. Inform.*, vol. 20, no. 4, pp. 6266–6279, Apr. 2024.

[22] X. Zhang and Z. Li, "Sliding-mode observer-based mechanical parameter estimation for permanent magnet synchronous motor," *IEEE Trans. Power Electron.*, vol. 31, no. 8, pp. 5732–5745, Mar. 2016.

[23] S. Tang, T. Shi, Y. Cao, Z. Lin, Z. Wang, and Y. Yan, "Simultaneous identification of load torque and moment of inertia of PMSM based on variable structure extended sliding mode observer," *IEEE Trans. Power Electron.*, vol. 39, no. 7, pp. 8585–8596, Jul. 2024.

[24] C. Yang, B. Song, Y. Xie, and X. Tang, "Online parallel estimation of mechanical parameters for PMSM drives via a network of interconnected extended sliding-mode observers," *IEEE Trans. Power Electron.*, vol. 36, no. 10, pp. 11818–11834, Oct. 2021.

[25] C. Lian, F. Xiao, S. Gao, and J. Liu, "Load torque and moment of inertia identification for permanent magnet synchronous motor drives based on sliding mode observer," *IEEE Trans. Power Electron.*, vol. 34, no. 6, pp. 5675–5683, Jun. 2019.

[26] I. Awaya, Y. Kato, I. Miyake, and M. Ito, "New motion control with inertia identification function using disturbance observer," in *Proc. Int. Conf. Ind. Electron., Control, Instrum., Automat.*, 1992, pp. 77–81.

[27] L. Niu, D. Xu, M. Yang, X. Gui, and Z. Liu, "On-line inertia identification algorithm for PI parameters optimization in speed loop," *IEEE Trans. Power Electron.*, vol. 30, no. 2, pp. 849–859, Feb. 2015.
[28] C. Yang, B. Song, Y. Xie, S. Lu, and X. Tang, "Stable simultaneous inertia and disturbance torque identification for SPMSM drive systems subject to mismatched rotor flux linkage," *IEEE J. Emerg. Sel. Topics Power Electron.*, vol. 10, no. 2, pp. 2445–2462, Apr. 2022.
[29] G. Zhang, G. Wang, D. Xu, and N. Zhao, "ADALINE-network-based PLL for position sensorless interior permanent magnet synchronous motor drives," *IEEE Trans. Power Electron.*, vol. 31, no. 2, pp. 1450–1460, Feb. 2016.

Yuanming Huang received the B.S. degree in electrical engineering and automation from Northeast Forestry University, Harbin, China, in 2021, and the M.S. degrees in electrical engineering in 2023 from Harbin Institute of Technology, Harbin, China, where he is currently working toward the Ph.D. degree in power electronics and electrical drives.

His current research interests include parameter identification and self-tuning technology of PMSM drives.

Guoqiang Zhang (Senior Member, IEEE) received the B.S. degree in electrical engineering from Harbin Engineering University, Harbin, China, in 2011, and the M.S. and Ph.D. degrees in electrical engineering from Harbin Institute of Technology, Harbin, China, in 2013 and 2017, respectively.

Since 2017, he has been with the Department of Electrical Engineering, Harbin Institute of Technology, where he is currently a Professor. His current research interests include control of electrical drives, and parameter identification technique, with main focus on sensorless field-oriented control of synchronous motor drives.

Dr. Zhang is currently an Associate Editor for *Journal of Power Electronics*.

Gaolin Wang (Senior Member, IEEE) received the B.S., M.S., and Ph.D. degrees in electrical engineering from Harbin Institute of Technology, Harbin, China, in 2002, 2004 and 2008 respectively.

In 2009, he was a Lecturer with the Department of Electrical Engineering, Harbin Institute of Technology, where he has been a Full Professor of electrical engineering since 2014. From 2009 to 2012, he was a Postdoctoral Fellow with Shanghai Step Electric Corporation, where he was involved in the traction machine control for direct-drive elevators. He has authored more than 60 technical papers published in IEEE Transactions. He is the holder of 30 Chinese patents. His current major research interests include permanent magnet synchronous motor drives, position sensorless control of ac motors, and digital control of power converters.

Dr. Wang is a Guest Associate Editor for IEEE TRANSACTIONS ON INDUSTRIAL ELECTRONICS, an Associate Editor for IEEE TRANSACTIONS ON TRANSPORTATION ELECTRIFICATION, *IET Electric Power Applications*, and *Journal of Power Electronics.*

Qiwei Wang (Member, IEEE) received the B.S., M.S., and Ph.D. degrees in electrical engineering in 2015, 2017, and 2022, respectively, from the Harbin Institute of Technology, Harbin, China, where he is currently working toward the Postdoc in power electronics and electrical drives with the School of Electrical Engineering and Automation.

His current research interests include parameter identification technique, and PMSM position sensorless control.

Siqi Wang received the B.S. and M.S. degrees in electrical engineering from the Nanjing University of Aeronautics and Astronautics, Nanjing, China, in 2018 and 2021, respectively. He is currently working toward the Ph.D. degree in power electronics and electrical drives with the Harbin Institute of Technology, Harbin, China.

His current research interests include advanced control of permanent magnet synchronous motor drive and position sensorless control of ac motors.

Dianguo Xu (Fellow, IEEE) received the B.S. degree in control engineering from the Harbin Engineering University, Harbin, China, in 1982, and the M.S. and Ph.D. degrees in electrical engineering from the Harbin Institute of Technology (HIT), Harbin, China, in 1984 and 1989, respectively.

In 1984, he was with the Department of Electrical Engineering, HIT, as an Assistant Professor. Since 1994, he has been a Professor with the Department of Electrical Engineering, HIT. He was the Dean of the School of Electrical Engineering and Automation, HIT, from 2000 to 2010, and an Assistant President from 2010 to 2014. He is currently the Vice President of the HIT. He authored or co-authored more than 600 technical papers. His research interests include renewable energy generation technology, power quality mitigation, sensorless vector-controlled motor drives, and high-performance PMSM servo system.

Dr. Xu is the Chairman of IEEE Harbin Section, the Co-EIC for IEEE TRANSACTIONS ON POWER ELECTRONICS, an Associate Editor for IEEE TRANSACTIONS ON INDUSTRIAL ELECTRONICS, IEEE JOURNAL OF EMERGING AND SELECTED TOPICS IN POWER ELECTRONICS. He was the recipient of the 2018 IEEE IAS Outstanding Achievement Award.